Table of Contents

Contents

Experimental Procedures

Materials Synthesis

Synthesis of $KCrSe_2$ was carried out on a 400 mg scale with handling of the reagents and products inside an argon-filled glove box (MBraun, <0.1 ppm of O_2). Stoichiometric amounts of Cr powder (Alfa Aesar, 99.94 %, -200 mesh, metal basis) and Se shots (Alfa Aesar, 99.99 %, metal basis) were loaded into a Pyrex insert together with K metal (Alfa Aesar, 99.9 %, metal basis). The insert was placed inside a Pyrex ampoule and sealed under vacuum with a blow torch. The ampoule was then placed upright in a muffle box furnace (Lenton) and heated at 250°C (1°C min^{-1} ramp) for 4 hours. The temperature was then raised to 600°C (1°C min^{-1} heating ramp, 72 h dwell, 5°C min^{-1} cooling). The sample was then taken out of the ampoule, ground using mortar and pestle, sealed under vacuum again and further reannealed at 600°C (1°C min^{-1} heating ramp, 48 h dwell, 5°C min^{-1} cooling ramp).

The synthesis of $KCrSe_2$-G10 involved employing the same procedure, with the incorporation of 10 wt.% graphite powder (Alfa Aesar, -100 mesh, 99.9995 %, metal basis) into the initial reaction mixture.

$CrSe_2$ and $CrSe_2$-G10 were prepared by the deintercalation of $KCrSe_2$ and $KCrSe_2$-G10 powders with iodine in acetonitrile solution respectively. Typically, inside an argon-filled glove box (MBraun, <0.1 ppm of O_2), 200 mg of $KCrSe_2$ powder was loaded into a round bottom flask (equipped with a stirring bar). The flask was attached to a Schlenk line and ca. 4 mL (given in excess) of 0.5 M iodine in acetonitrile solution (Alfa Aesar, anhydrous, 99.8 %) was added under N_2 flow. The mixture was stirred 24 hours at ambient temperature (ca. 21°C). The product was then filtered in air resulting in a black powder on the filter. The powder was washed with 100 ml of acetonitrile, then with excess of deionised water, finally rinsed with 100 ml of ethanol and left to dry overnight in an evacuated desiccator.

Chemical stability of $CrSe_2$ in aqueous electrolytes

Chemical stability tests of $CrSe_2$ were carried out by dispersing 40 mg of $CrSe_2$ in 10 mL of either 1M KOH, 1M H_2SO_4, 1M Li_2SO_4, or 1M Na_2SO_4 aqueous solutions. The respective dispersion was left stirred for 24 hours at 20 ºC in ambient. The product was then filtered, washed with deionized water, and dried in a desiccator under vacuum overnight.

Powder X-ray diffraction (PXRD)

Non-air-sensitive samples were measured on a Rigaku MiniFlex 6G diffractometer ($CuK_{\alpha 1}$ and $CuK_{\alpha 2}$ wavelengths - 1.5406 and 1.5444 Å respectively) equipped with a D/teX Ultra detector operating in the Bragg–Brentano geometry. Powder samples were carefully packed onto zero background holders and levelled using a glass microscope slide. SC electrodes were also tested by attaching them directly to the holder with a double-sided tape. Diffraction patterns were collected with a step size of 0.015° and time per step of 1° min^{-1}. The sample holder was spined during the measurements at 10 rpm.

PXRD measurements of air-sensitive samples, $KCrSe_2$ and $KCrSe_2$ (10 wt. % graphite), were performed on a PANalytical Empyrean diffractometer ($CuK_{\alpha 1}$ and $CuK_{\alpha 2}$ wavelengths - 1.5406 and 1.5444 Å respectively) operating in the Debye-Scherrer geometry. The samples were packed inside an Ar-filled glove box (MBraun, <0.1 ppm O_2) into 0.5 mm diameter (0.1 mm wall thickness) No.50 special glass capillaries (Hilgenberg), which were sealed with a blow torch. The PXRD patterns were collected with a step size of 0.016° and time per step of 5° min^{-1}. To enable a proper comparison with simulated diffraction patterns the background of $KCrSe_2$ and $KCrSe_2$-G10 was subtracted in the Highscore Plus Software (Panalytical).

SUPPORTING INFORMATION

Le Bail refinement of selected PXRD data was performed using GSAS-II software. [1] The refined parameters included unit cell parameters, sample displacement, strain, and crystallite broadening. Background was fitted using shifted Chebyshev polynomic shape.

All datasets were plotted using the Origin 2020 software.

Raman spectroscopy

Raman spectra of all samples were collected in a backscattering configuration on a Horiba JY HR800 spectrometer with a 532 nm laser excitation wavelength (laser power without any filters 50 mW) and a 600 groves mm^{-1} grating. The spectra were acquired using a 50× objective. As the samples were found to degrade in air in the laser beam, to prevent them from oxidation in air, they were loaded into capillaries (0.5 mm diameter, 0.1 mm wall thickness) in an Ar-filled glove box (MBraun, <0.1 ppm O_2) and sealed with a blow torch. The optimized accumulation time was 10s and laser intensity was adjusted to 10% of the full power (corresponding 5 mW).

Scanning electron microscopy (SEM) coupled with the Energy dispersive X-ray Spectroscopy (EDXS)

The powders were immobilized on the holders using carbon stickers. SEM measurements were carried out on Phillips XL30 SEM instrument coupled with an Oxford Instruments X-act spectrometer for EDXS analysis using INCA software. Prior the EDXS measurements, it was calibrated with a Cu standard.

Transmission electron microscopy (TEM) coupled with Energy dispersive X-ray Spectroscopy (EDXS)

For nanoscale structure and chemical analysis by transmission electron microscopy (TEM), the $CrSe_2$ crystalline powders were grinded, suspended in butanol and transferred to C-lacey Cu-grids by drop-casting. TEM investigation was performed on a JEOL (JEM200F) NEOARM instrument operated at 200 kV. Chemical analysis was conducted on multiple crystals by energy-dispersive X-ray spectroscopy mapping with a dual silicon drift detector (combined 200 mm^2) system in scanning TEM mode. High-resolution (HRTEM) micrographs were Fourier filtered by a radiance difference filter cutting higher frequency noise contributions beyond the maximum image resolution using the lite version of the DigitalMicrograph plug-in 'HREM-Filters Pro/Lite v.4.2.1' (HREM Research Inc.).

X-ray photoelectron spectroscopy (XPS)

XPS was carried on a Scienta 300, operating at or below 1x10^{-9} mbar. The X-ray source was a SPECS monochromated Al K$_\alpha$ source (photon energy 1486.6eV) operating at approx. 12 KV and 200 watts power. The instrument maintained a pass energy set to 150 eV for all spectra. High resolution spectra were based on 2 to 16 scans depending on quality of data, a dwell time of 533 ms and a step size of 20 meV. The FWHM of the Ag 3d5 peak at 368.4eV was routinely below 0.7eV with a similar value for Au 4f7 at 84 eV and experimental drift as a function of time is negligible over a period of 24 hours. All data analysis and fitting were done in the CasaXPS software. The resulting plots then were plotted using the Origin 2020 software.

Supercapacitor ink preparation

The active material dispersion was prepared by mixing 6 mg of $CrSe_2$, 15 µL of Nafion (Sigma-Aldrich, 5 wt. % in mixture of lower aliphatic alcohols and water, contains 45% water) and 185 µL dimethylformamide (Sigma-Aldrich, ACS reagent). The mixture was sonicated in a closed vial for 10 minutes to achieve a uniform dispersion. 4 µL of the dispersion was dropped on a clean 1 cm × 0.7 cm Ti foil electrode and left to dry overnight at room temperature.

Electrochemical measurements in a three-electrode system

Electrochemical measurements were carried out on Biologic Essential Potentiostat SP-150. The three-electrode system was used consisting of working electrode with the sample on the Ti foil (1 cm × 0.7 cm) as working electrode, 1×1 cm Pt foil as a counter electrode and Ag/AgCl (3M NaCl) as a reference electrode. Cyclic voltammetry was carried out at the 5, 20, and 50 mV s^{-1} rate. Galvanostatic charge - discharge measurements were done at 0.2 and 0.4 mA respectively.

N2-gas adsorption measurements

Gas sorption isotherms were measured using a Quadrasorb Evo gas sorption analyser (Anton Parr). Samples were loaded into an ampoule with a 9 mm diameter bulb at the end and degassed under vacuum at 60°C for 16 hours. The experiments were performed at 77 K using nitrogen as adsorbate gas and analysis was performed using Quadrawin software suite. Brunauer Emmett Teller (BET) theory was used to deduct the specific surface areas from the isotherms.

DFT calculations

To calculate the electronic structure of the investigated materials, on $CrSe_2$, we have performed quantum mechanical simulations based on the Density Functional Theory (DFT). Drawing upon previous studies, $CrSe_2$ has been identified as a magnetic compound, therefore the influence of the magnetic ordering of the electronic structure was taken into the account. [2] The simulations were performed in the Quantum Atomistix ToolKit (QuantumATK) 2022.03 package using an exchange-correlation functional with polarized spin based on the linear combination of atomic orbitals framework by employing the Perdew−Burke−Ernzerhof functional. [3] To define the numerical accuracy, the density mesh cut off of 30 Hartree was introduced. The iteration tolerance and force tolerance were set to 1×10^{-4} eV and 0.02 eV $Å^{-1}$ respectively. Simulation of

weak van der Waals forces between $[CrSe_2]$ layers was performed using the DFT-D3 dispersion scheme. We have applied Monkhorst–Pack sampling for integration in the Brillouin zone with $9 \times 9 \times 5$ k-points for structure optimization and $15 \times 15 \times 8$ k-points for DFT calculation.

Results and Discussion
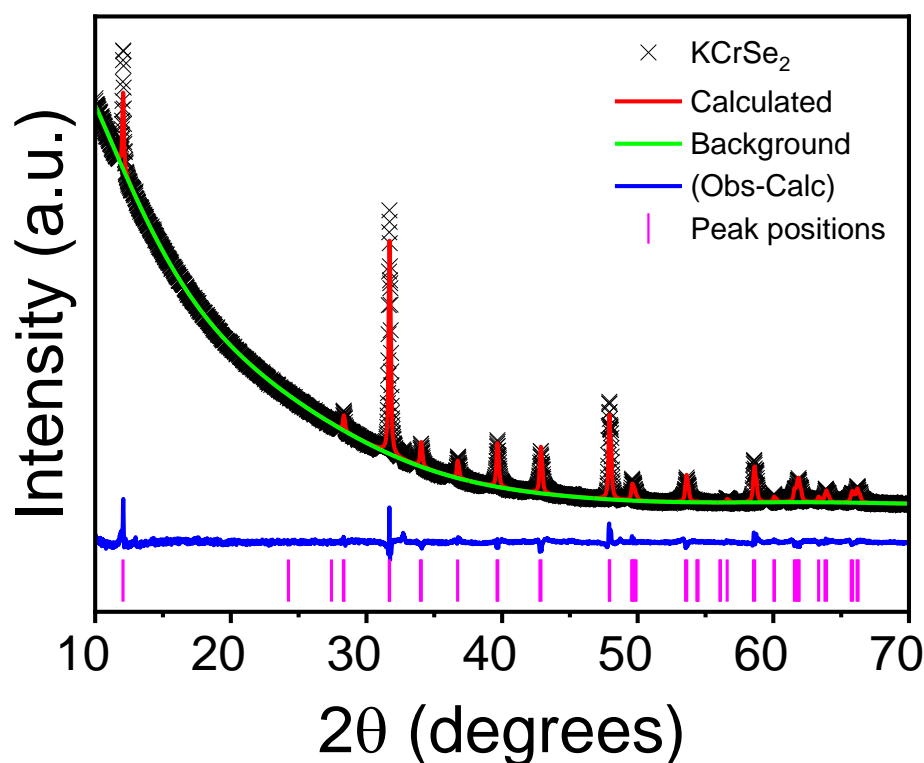
Figure S1. LeBail refinement of the experimental PXRD profile (CuK_α) for a sample with a nominal composition $KCrSe_2$ against a structure model (Space group: *C*2/*m*). Measured data are shown as black crosses; the calculated profile is shown by a solid red line. The difference between the calculated and experimental data is shown as a blue profile. Magenta vertical bars represent the reflection positions for the phase.
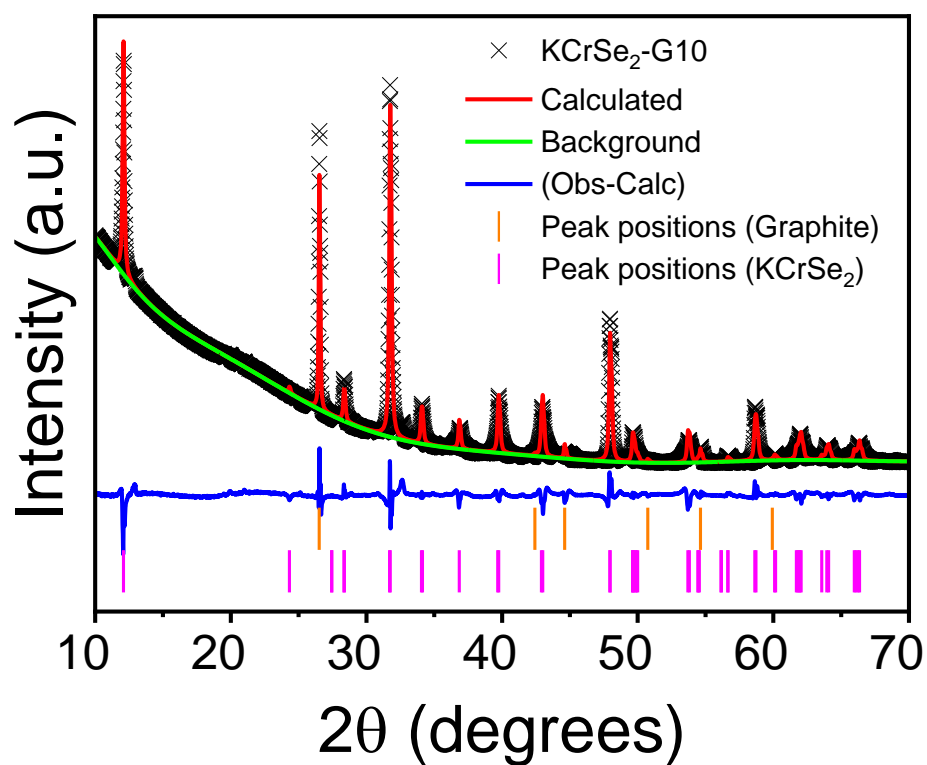
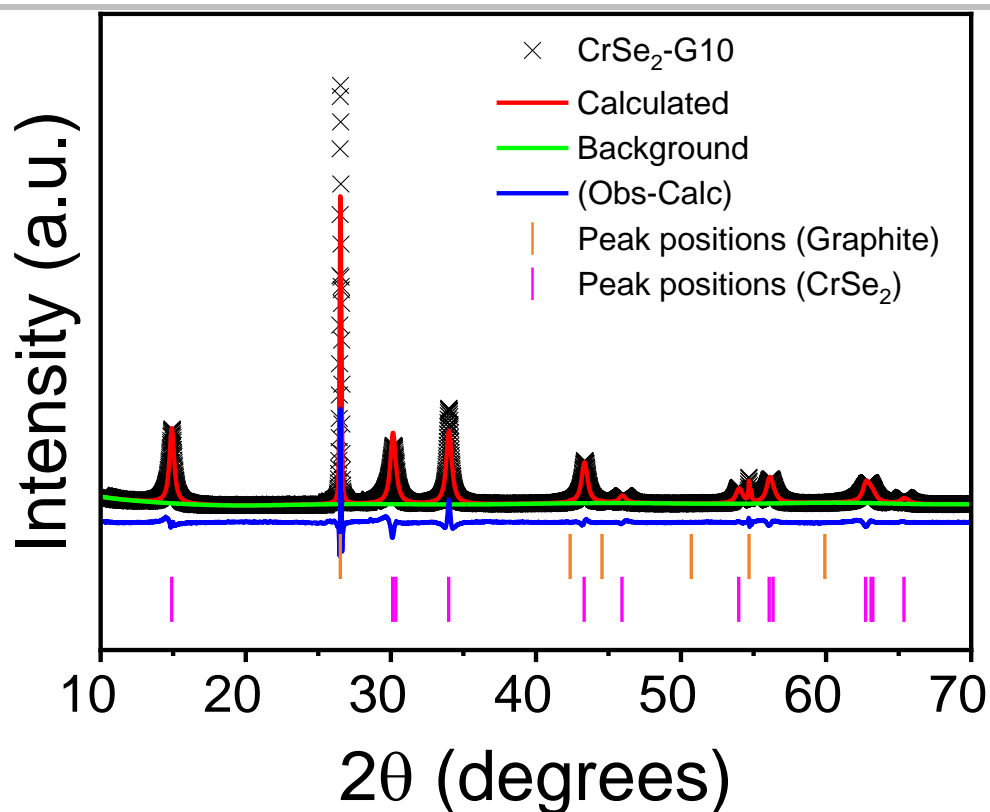**Figure S2**. LeBail refinement of the experimental PXRD profile (CuKα) for a sample with a nominal composition KCrSe$_2$ / 10 wt.% graphite against a structure models (Space group: $C2/m$ for KCrSe$_2$ and $P6_3/mmc$ for graphite). Measured data are shown as black crosses; the calculated profile is shown by a solid red line. The difference between the calculated and experimental data is shown as a blue profile. Magenta and orange vertical bars represent the reflection positions for the KCrSe$_2$ and graphite phases respectively.
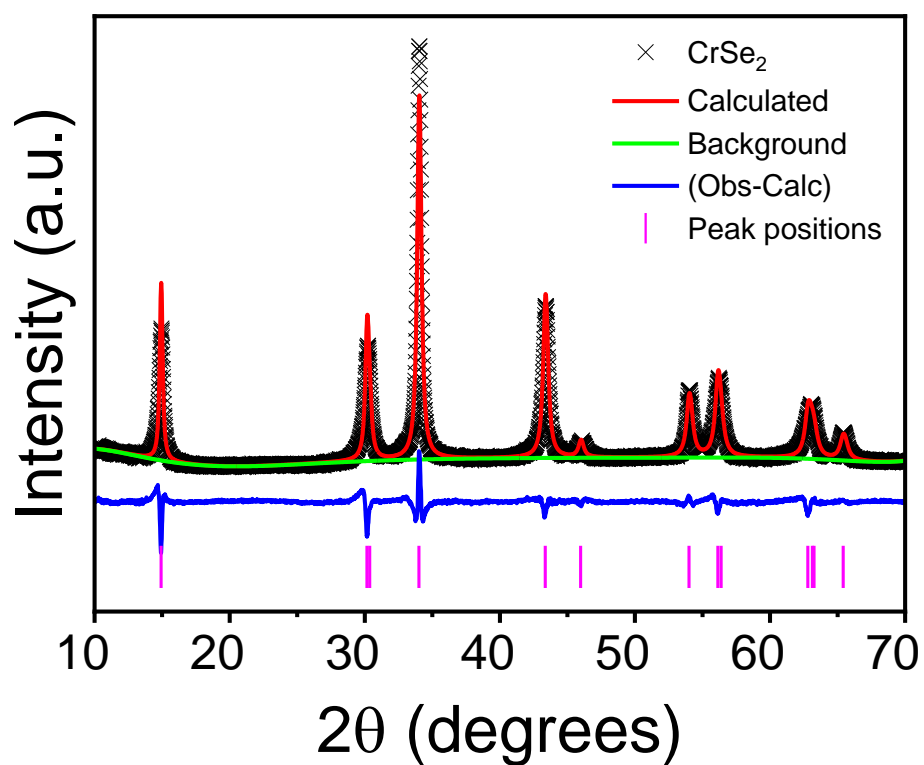
Figure S3. LeBail refinement of the experimental PXRD profile (CuK$_\alpha$) for the CrSe$_2$ sample prepared by deintercalation from KCrSe$_2$ with iodine against a CrSe$_2$ structure model (Space group: P-3m1). Measured data are shown as black crosses; the calculated profile is shown by a solid red line. The difference between the calculated and experimental data is shown as a blue profile. Magenta vertical bars represent the reflection positions for the phase.

Figure S4. LeBail refinement of the experimental PXRD profile (CuKα) for a $CrSe_2$-G10 sample prepared by deintercalation from $KCrSe_2$ containing 10 % of graphite with iodine against a $CrSe_2$ structure model (Space group: *P*-3*m*1 and *P*63/*mmc* for graphite). Measured data are shown as black crosses; the calculated profile is shown by a solid red line. The difference between the calculated and experimental data is shown as a blue profile. Magenta and orange vertical bars represent the reflection positions for the $CrSe_2$ and graphite phases respectively.
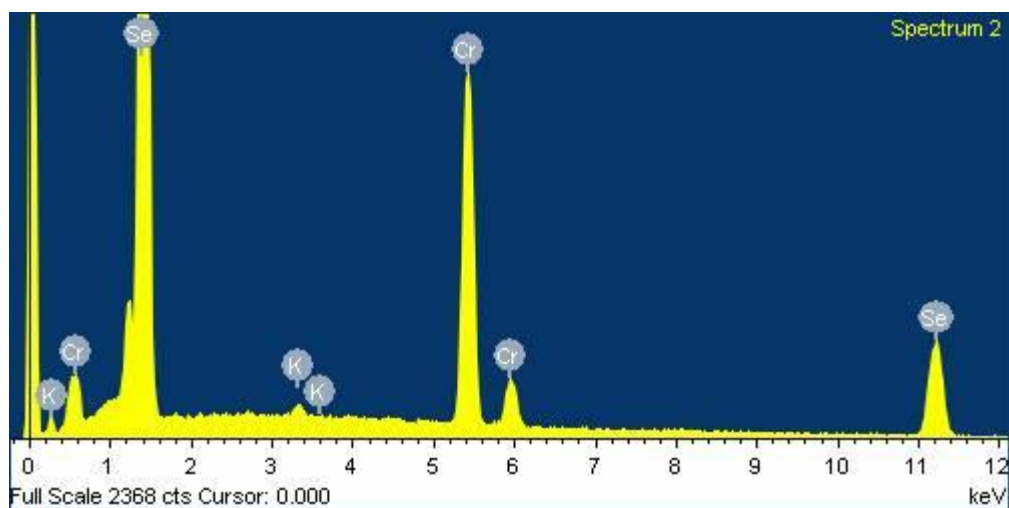
Figure S5. EDX spectrum of the $CrSe_2$ sample prepared by deintercalation from $KCrSe_2$ with iodine.
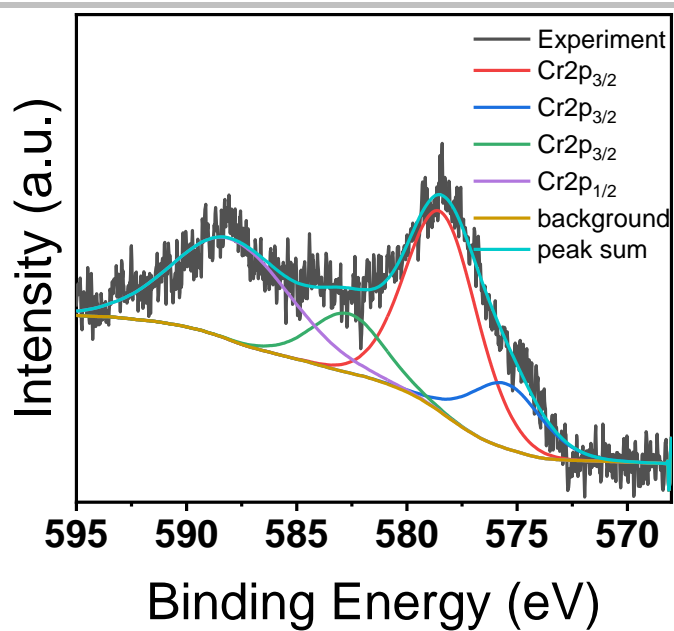
Figure S6. High resolution XP spectrum of Cr 2p in CrSe₂ sample prepared by deintercalation from KCrSe₂ with iodine. The main peaks assignment in the deconvoluted spectrum BE Cr 2p3/2 588.4 eV and BE Cr 2p1/2 at 578.6 eV.
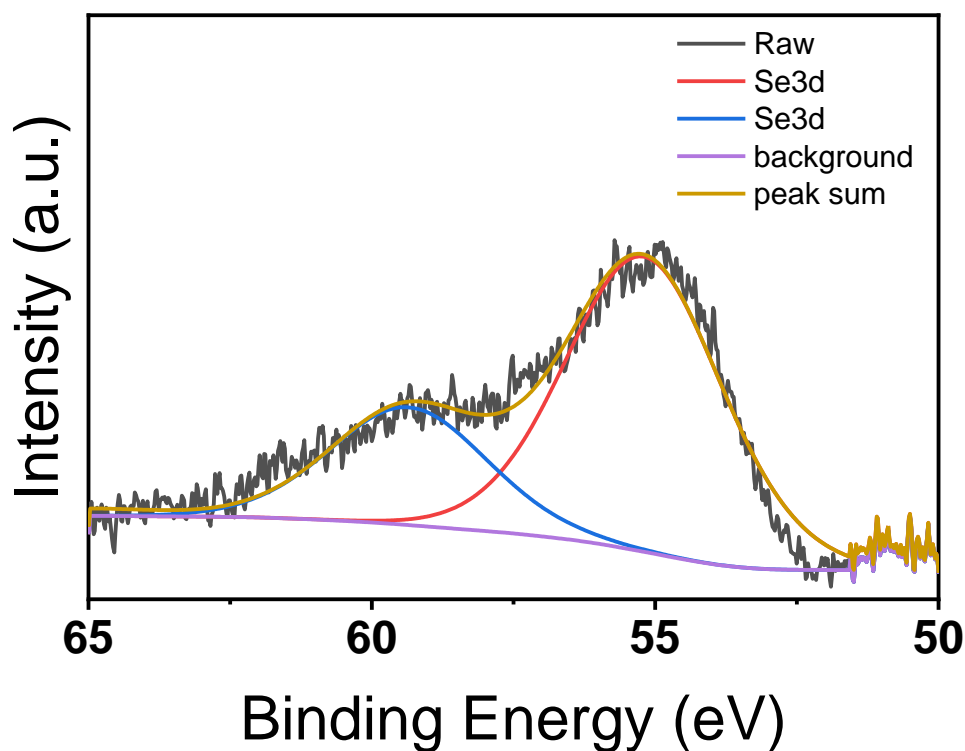
Figure S7. High resolution XP spectrum of Se 3d of CrSe₂ sample prepared by deintercalation from KCrSe₂ with iodine. The peaks assignment in the deconvoluted spectrum Se 3d peaks at BE Se 2d5/2 59.35 eV and Se 2d3/2 55.2 eV

a

c

SU8230 5.0kV 11.9mm x1.00k LA5(UL)   50.0μm

SU8230 5.0kV 11.9mm x1.00k LA5(UL)   50.0μm

b

d

SU8230 5.0kV 12.1mm x10.0k LA5(UL)   5.00μm

SU8230 5.0kV 11.9mm x10.0k LA5(UL)   5.00μm
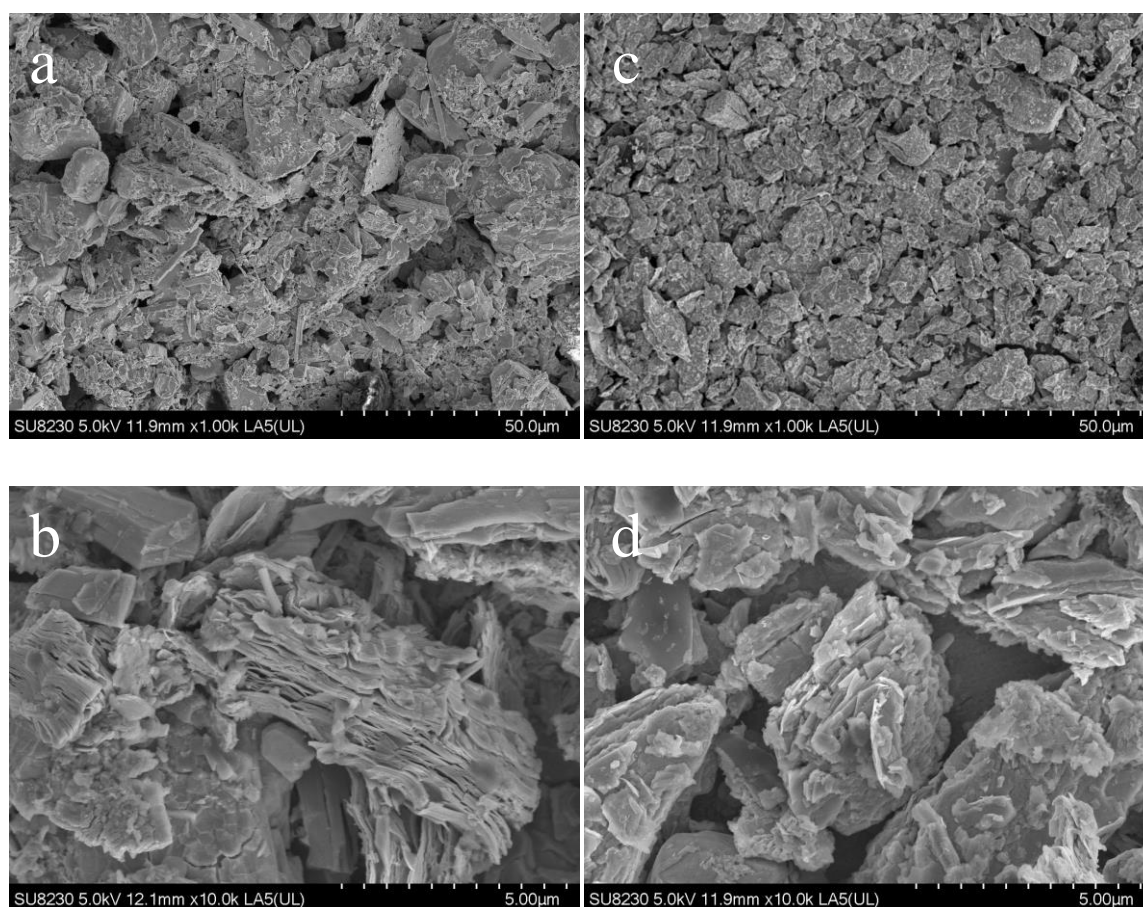
Figure S8. (a-b) SEM images of CrSe$_2$ sample prepared by deintercalation from KCrSe$_2$ with iodine and (c-d) of CrSe$_2$-G10 sample prepared by deintercalation from KCrSe$_2$ / 10 wt. % graphite with iodine.
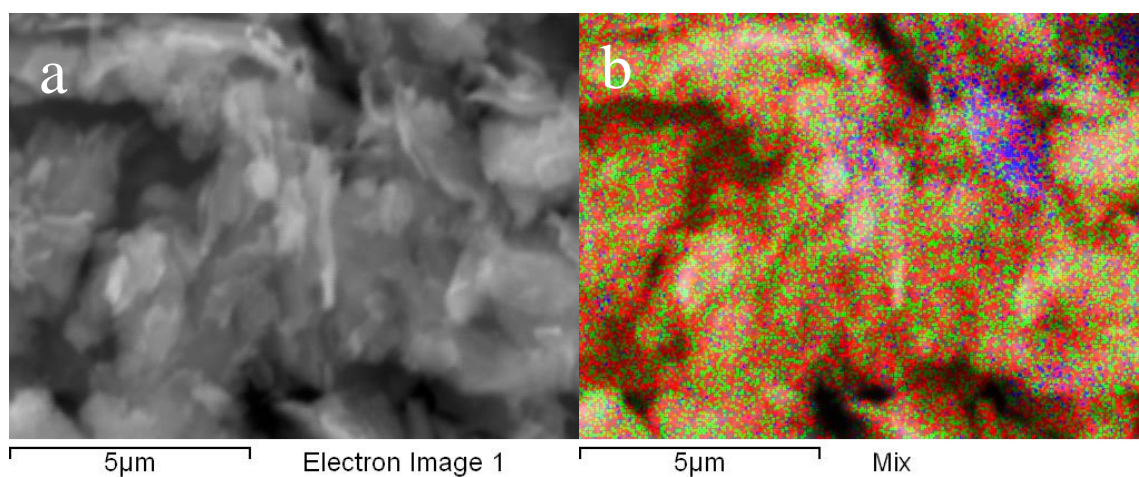
Figure S9. The distribution of graphite particles within the CrSe$_2$ matrix in CrSe$_2$-G10 sample prepared by deintercalation from KCrSe$_2$ / 10 wt. % graphite with iodine as illustrated by (a) SEM image and (b) the interposition of the relevant EDX maps for Cr, Se and C on the SEM image.
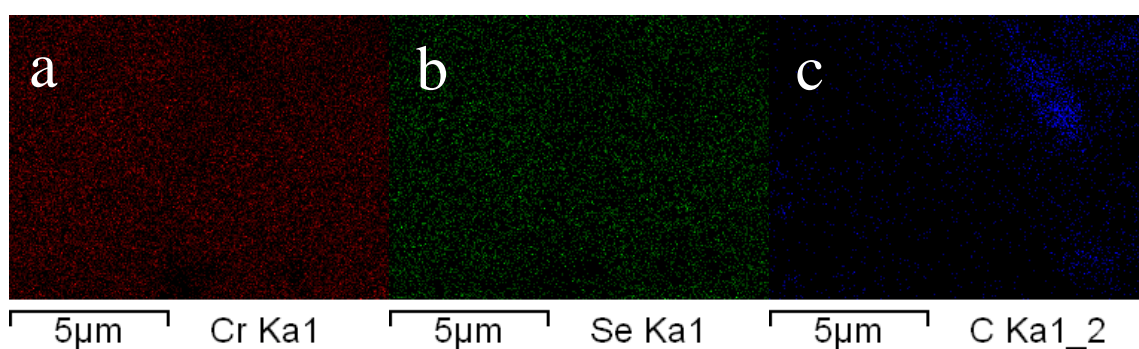
Figure S10. The individual EDX maps for Cr, Se and C in CrSe$_2$-G10 sample prepared by deintercalation from KCrSe$_2$ / 10 wt. % graphite with iodine.
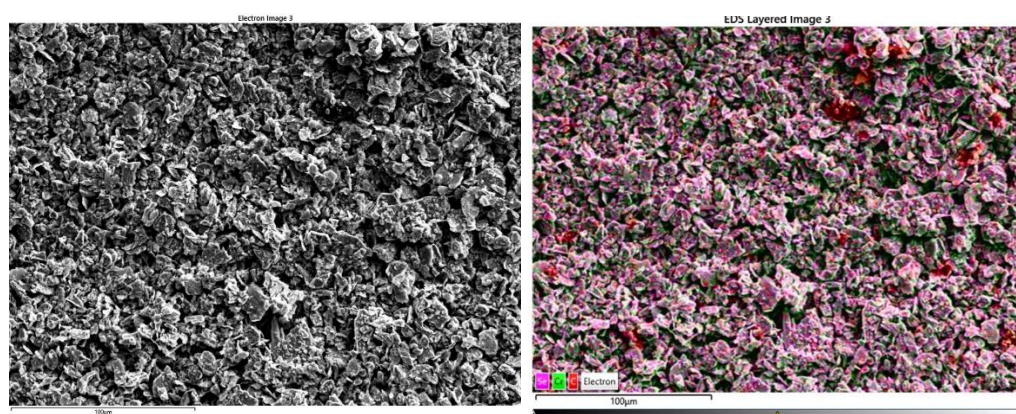
Figure S11. The distribution of graphite particles within the CrSe$_2$ matrix in CrSe$_2$-G10 sample prepared by deintercalation from KCrSe$_2$ / 10 wt. % graphite with iodine as illustrated by (a) SEM image and (b) the interposition of the relevant EDX maps for Cr, Se and C on the SEM image. The scale bar is 100 mm.

9
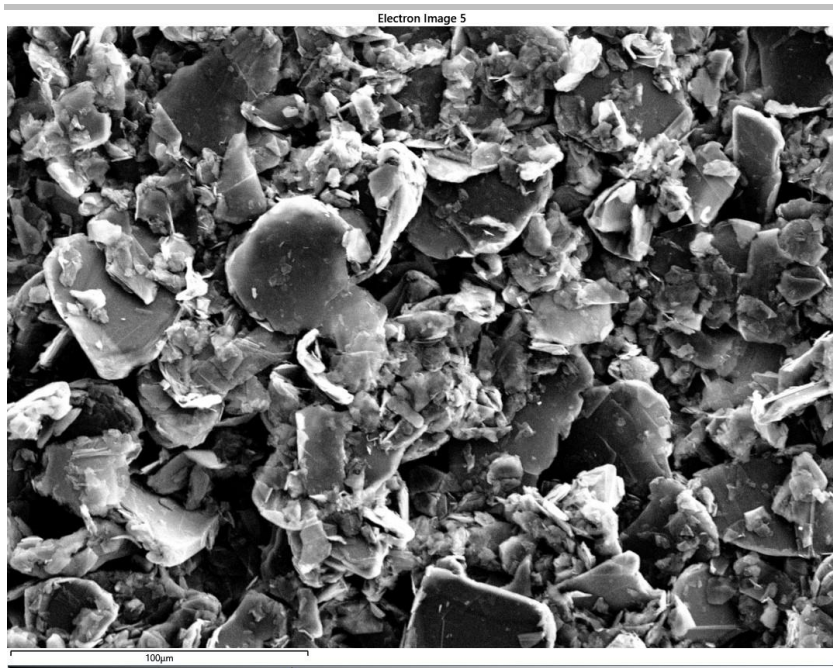
Figure S12. The SEM image of on the original graphite sample used in the synthesis of $CrSe_2$-G10 sample.
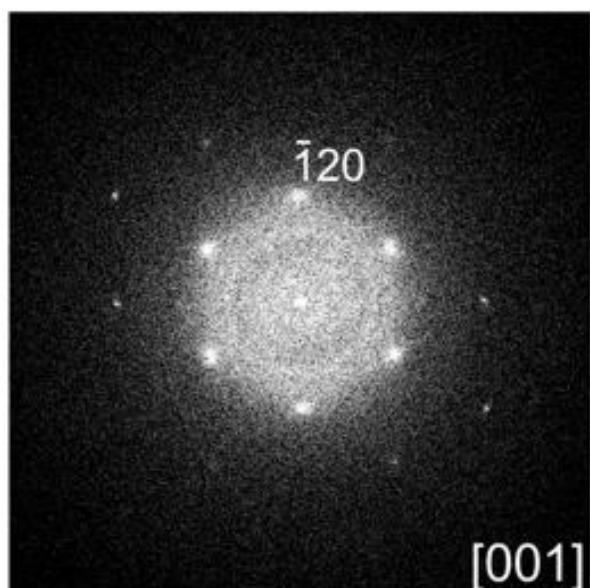
Figure S13. [001] SAED pattern of $CrSe_2$ sample prepared by deintercalation from $KCrSe_2$ graphite with iodine.
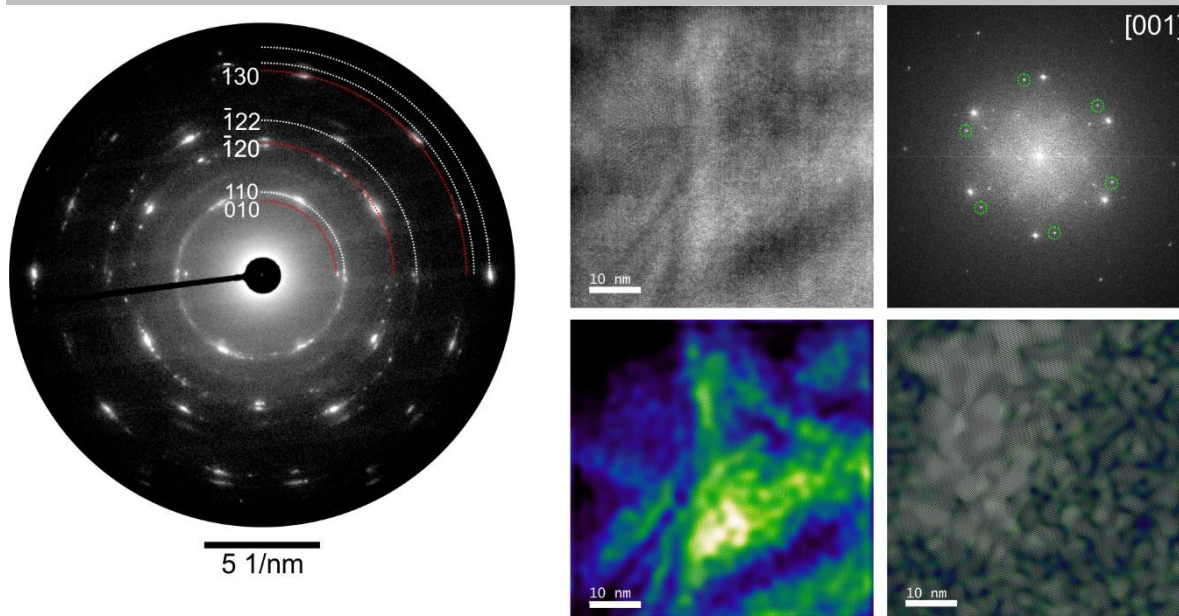
Figure S14. TEM investigation of $CrSe_2$ sample. (a) SAED pattern showing multiple crystalline orientations. The corresponding [001] zone reflections are distributed on the red-highlighted rings. (b) HRTEM analysis of in-plane rotated [001] crystal components as represented by an HRTEM micrograph, (c) FFT intensity pattern showing a second rotated component (green circled reflection) giving rise to weak six-fold dynamical diffraction intensities centered around main structure reflections. (d) Real-space location analysis by Fourier space-filtered inverse FFT using masks around the main intensities and (f) the circled secondary component intensities.
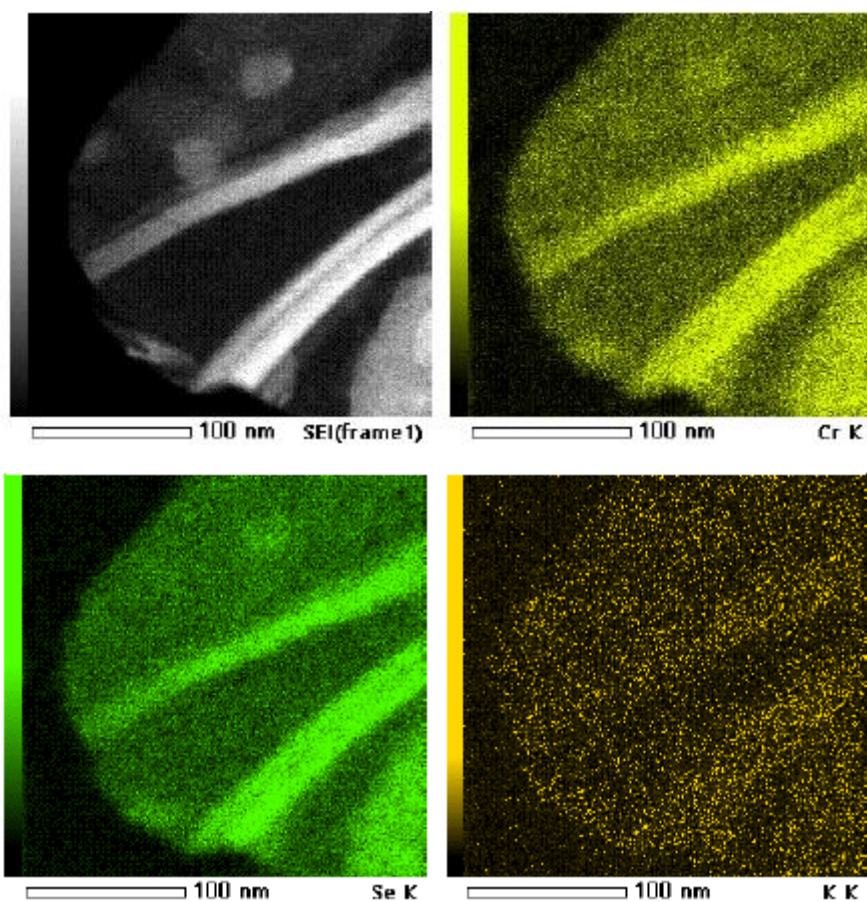
Figure S15. Energy dispersive X-ray (EDX) mapping analysis of $CrSe_2$ sample prepared by deintercalation from $KCrSe_2$ with iodine.
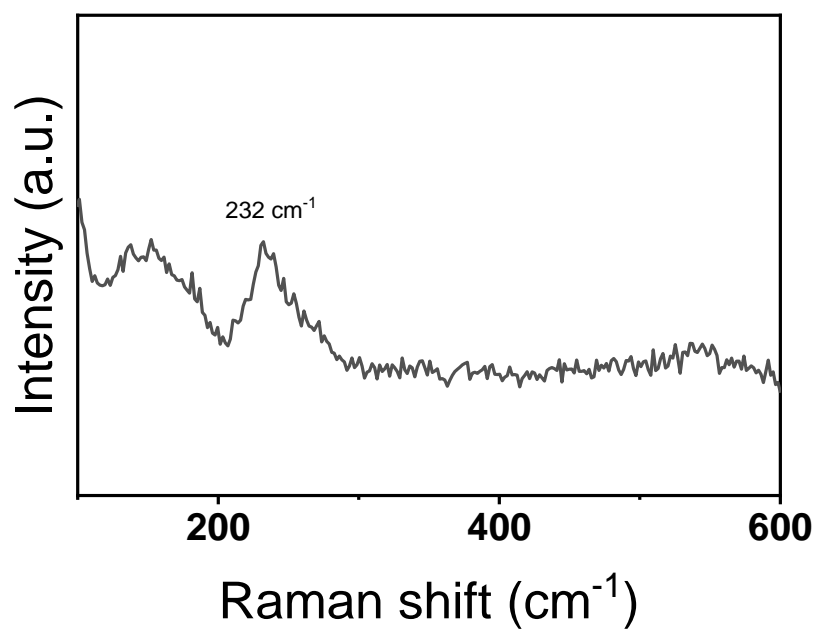
Figure S16. Raman spectrum of $CrSe_2$ prepared by deintercalation from $KCrSe_2$ with iodine (532 nm laser wavelength and 5 mW laser power).
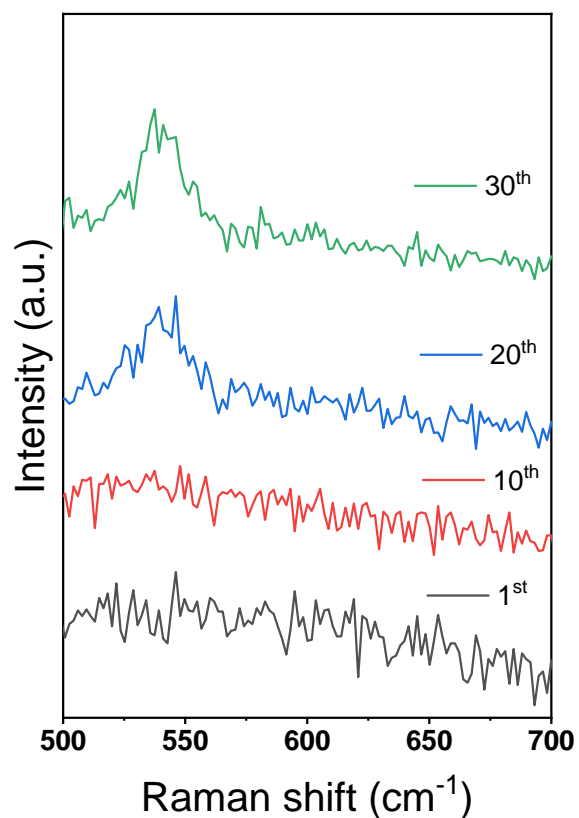
Figure S17. The effect of a prolonged exposure to the 5 mW laser beam on Raman spectra of the $CrSe_2$ sample prepared by deintercalation from $KCrSe_2$ with iodine at room temperature. The spectra are corresponding to the accumulations for 10s over 1, 10, 20 and 30 repetitions.
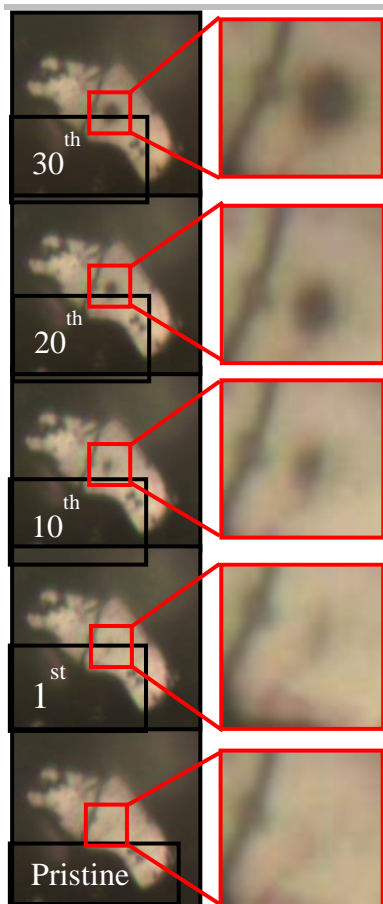
Figure S18. The effect of a prolonged exposure to the 5 mW laser beam on the surface of $CrSe_2$ sample prepared by deintercalation from $KCrSe_2$ with iodine. The optical images were recorded after the accumulations for 10s over 1, 10, 20 and 30 repetitions. The zoom area highlights a distinctive "beam burn" that appears at the surface upon the exposure.
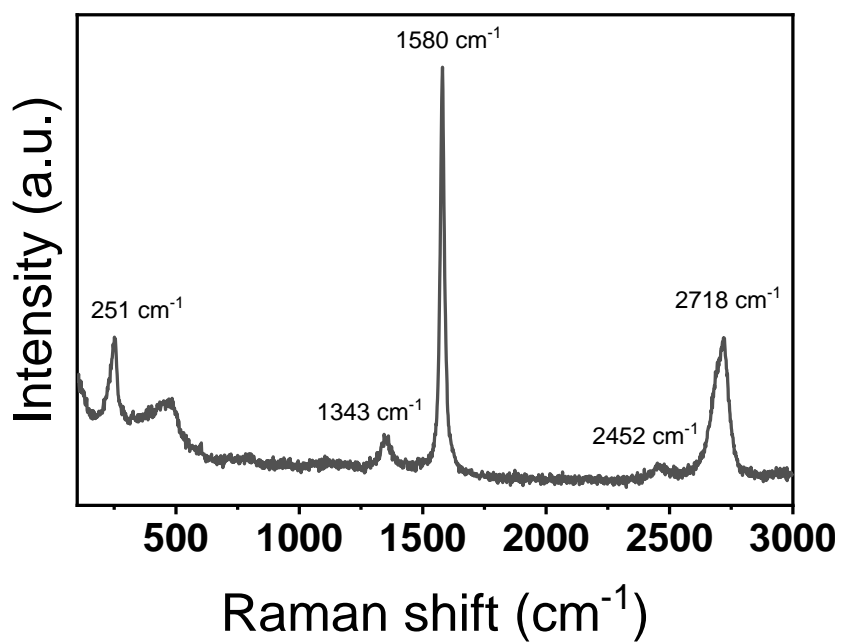
Figure S19. Raman spectrum of $CrSe_2$-K-G10 (532 nm laser wavelength and 5 mW laser power).
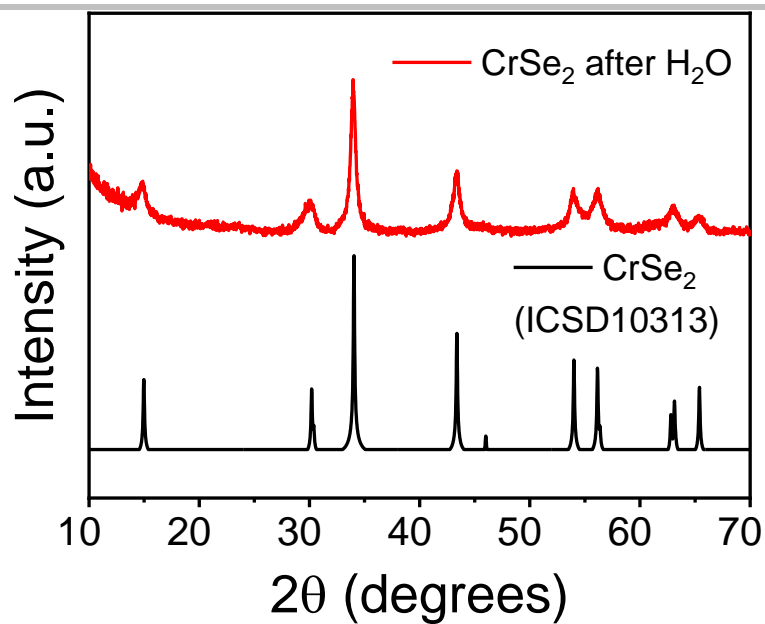
Figure S20. PXRD patterns of CrSe$_2$ after stirring in H$_2$O for 24 h at 20ºC (red) in comparison with CrSe$_2$ pattern calculated from ICSD No. 10313 (black).
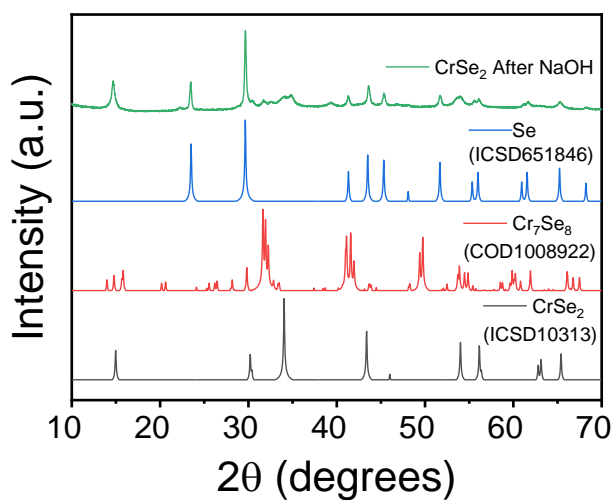
Figure S21. PXRD patterns of CrSe$_2$ before and after 24 hrs stirring in 1M KOH in comparison with simulated diffraction patterns for the potential products.
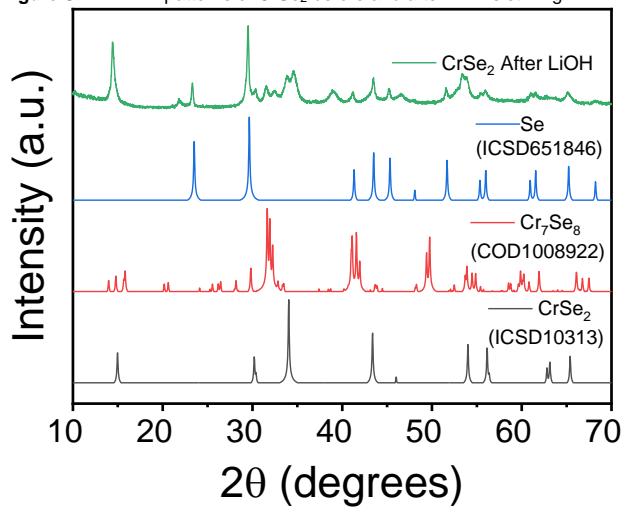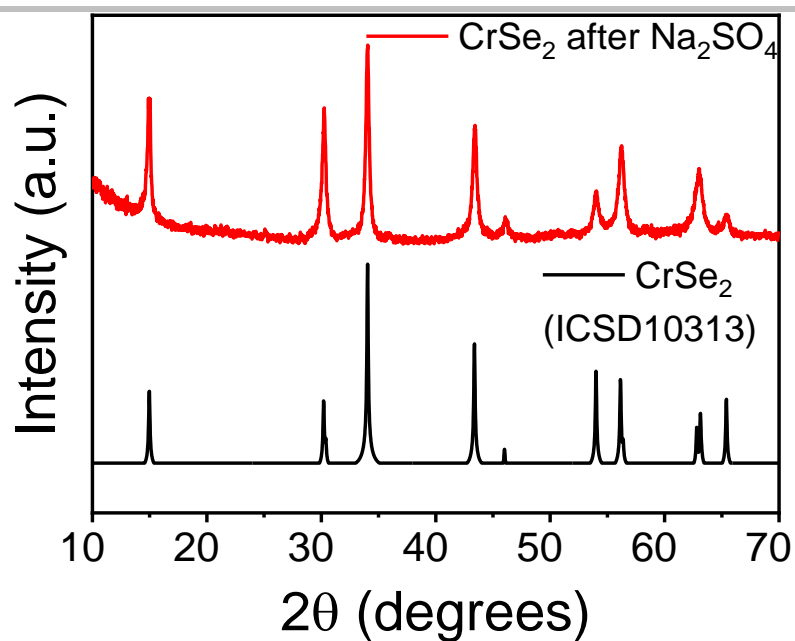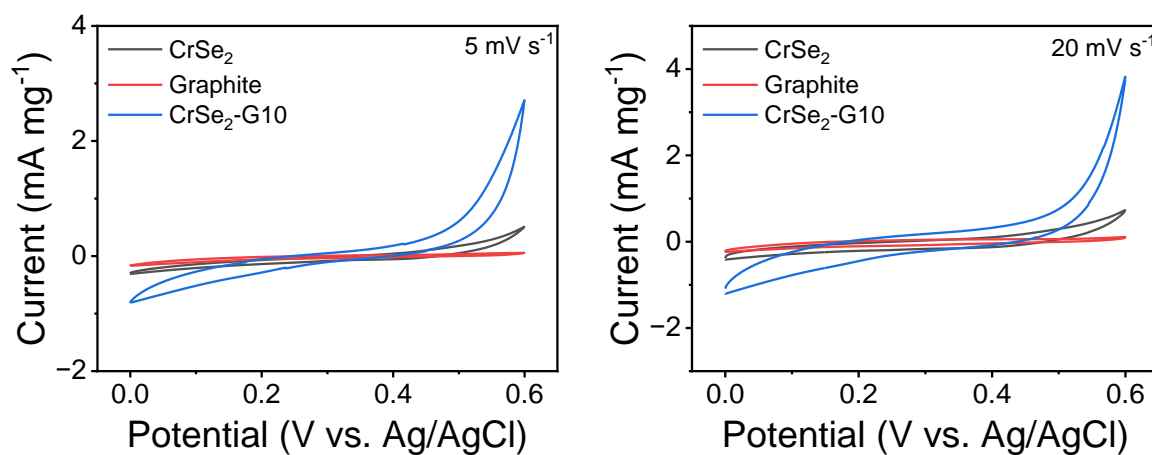

Figure S22. PXRD patterns of CrSe$_2$ before and after 24 hrs stirring in 1M KOH in comparison with simulated diffraction patterns for the potential products.

Figure S23 PXRD patterns of $CrSe_2$ after stirring in Na_2SO_4 for 24 h at 20ºC (red) in comparison with $CrSe_2$ pattern calculated from ICSD No. 10313 (black)

Figure S24. The CV curves of the supercapacitor test of $CrSe_2$, graphite and $CrSe_2$-G10 in three electrode system in 1M H_2SO_4 at 5 and 20 mV S^{-1}.
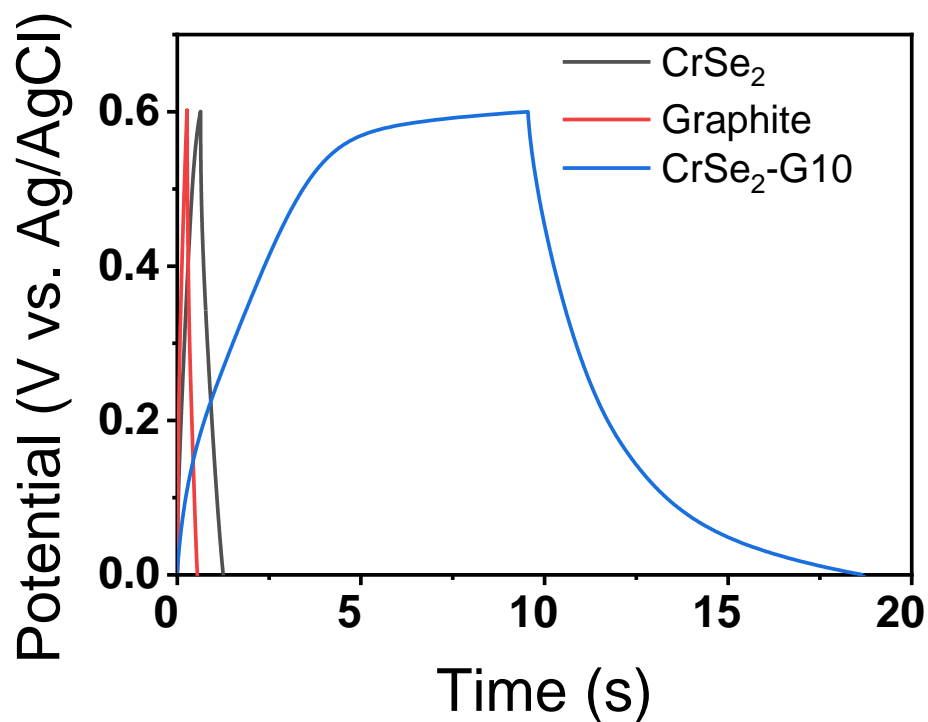
Figure S25. The GCD curves of the supercapacitor test of CrSe₂, graphite and CrSe₂-G10 in three electrode system in 1 M H₂SO₄ at 2 A g⁻¹.
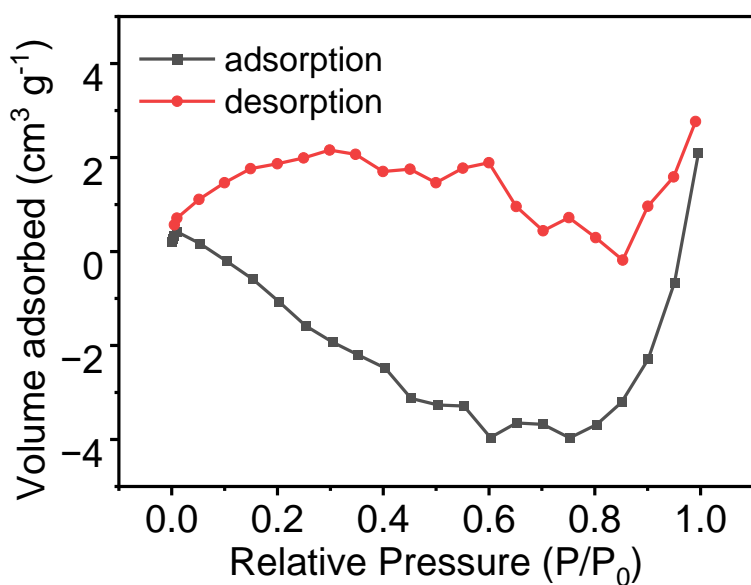

Figure S26. Nitrogen adsorption-desorption isotherms for CrSe₂ sample. The lack of traction between adsorption and desorption is due to complete inability of the system to collect a reasonable data due to the low surface area of the sample.
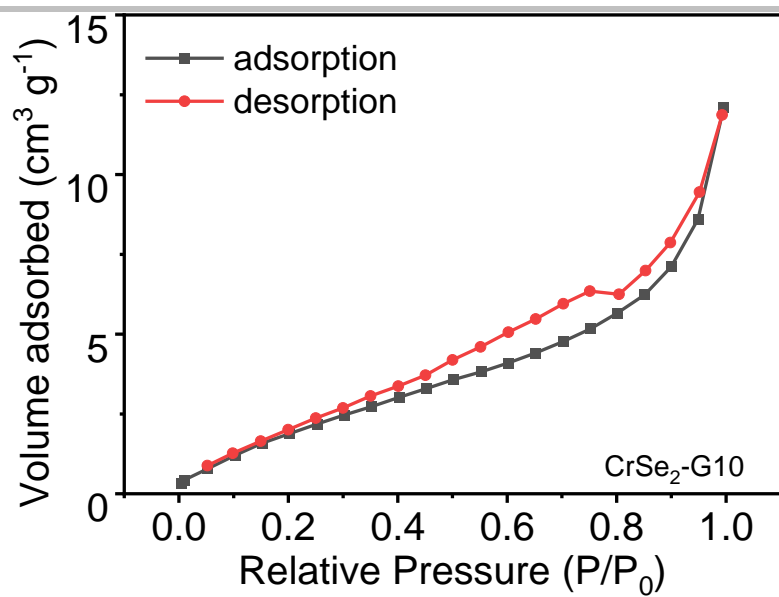
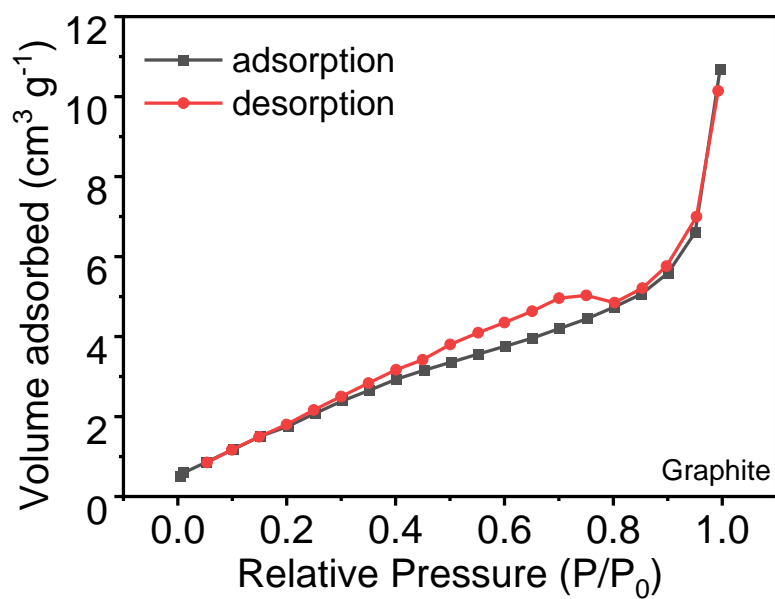**Figure S27.** Nitrogen adsorption-desorption isotherms for CrSe₂-G10.

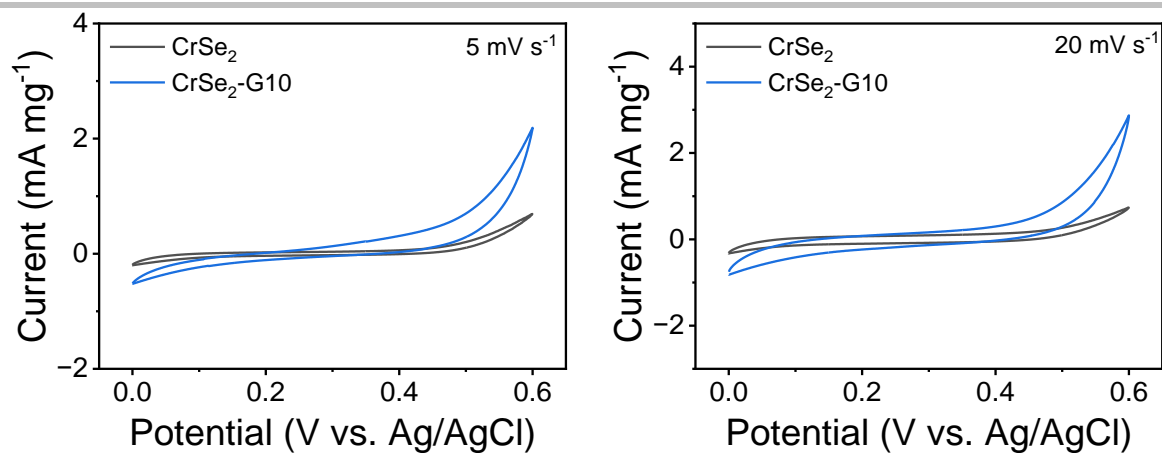**Figure S28.** Nitrogen adsorption-desorption isotherms for graphite.

Figure S29. The CV curves of the supercapacitor test of $CrSe_2$ and $CrSe_2$-G10 in three electrode system in 1 M Li_2SO_4 at 5 and 20 mV S^{-1}.
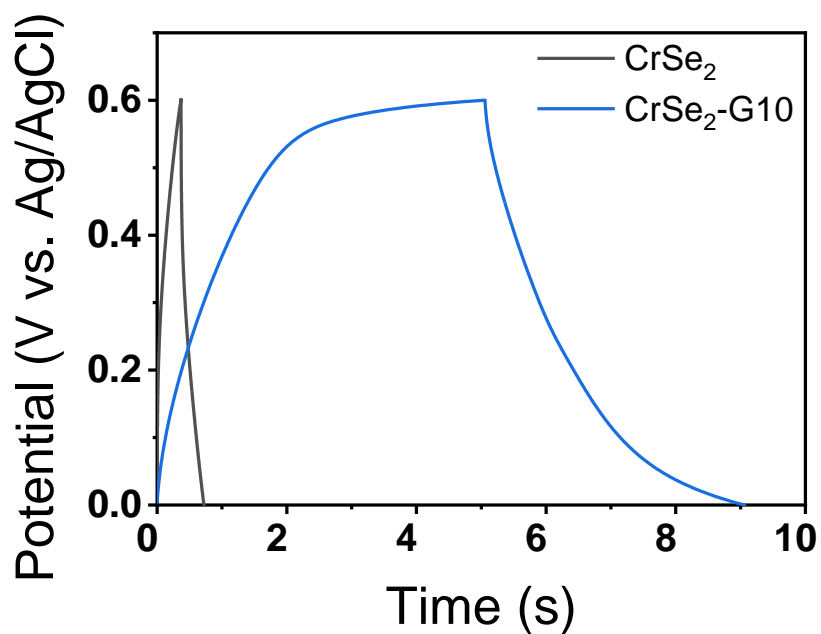
Figure S30. The GCD curves of the supercapacitor test of $CrSe_2$ and $CrSe_2$-G10 in three electrode system in 1M Li_2SO_4 at 2 A g^{-1}.

Figure S31. The CV curves of the supercapacitor test of $CrSe_2$ and $CrSe_2$-G10 in three electrode system in 1M Na_2SO_4 at 5 and 20 mV S^{-1}.
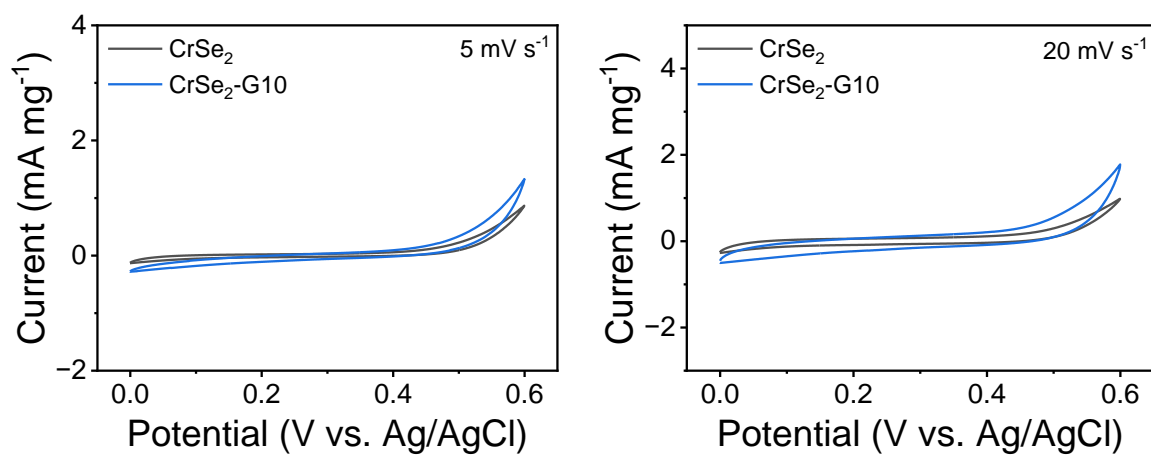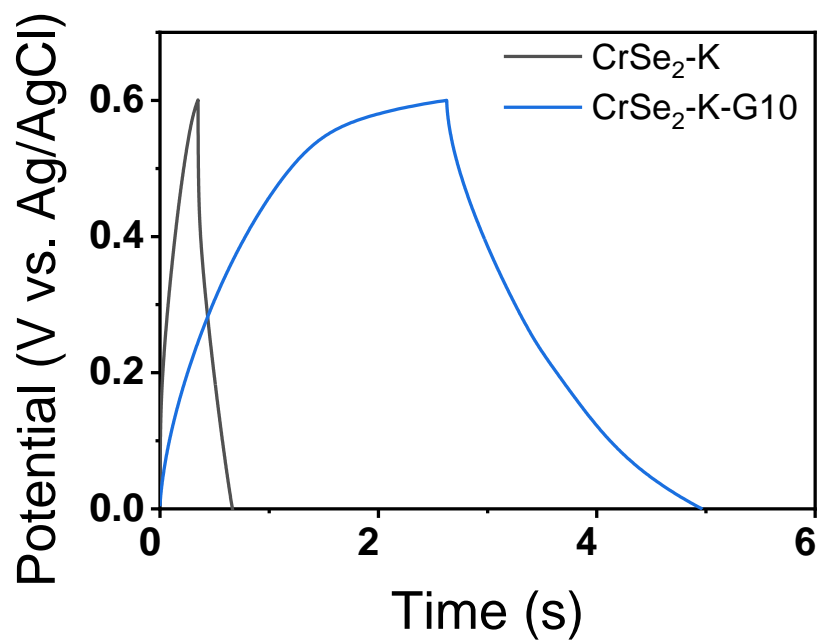
18

Figure S32. The GCD curves of the supercapacitor test of $CrSe_2$ and $CrSe_2$-G10 in three electrode system in 1 M Na_2SO_4 at 2 A g^{-1}.
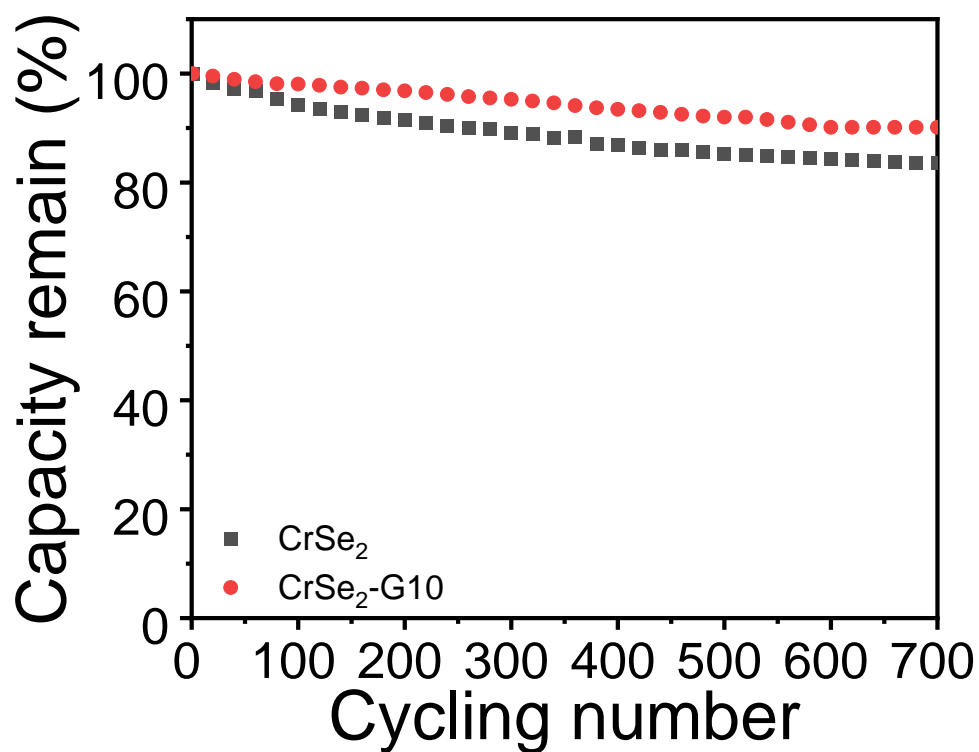

Figure. S33. The long-term stability of pristine $CrSe_2$ and $CrSe_2$-G10 samples under high current density of 2 A g^{-1}.
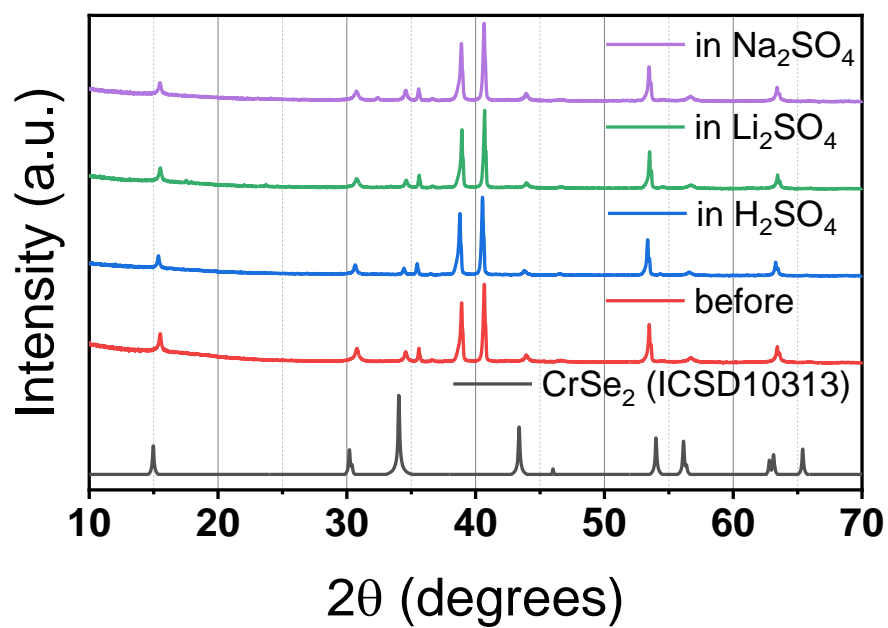
Figure S34. Stability examination of carbon CrSe$_2$ electrode ink dropped on the Ti Foil before and after supercapacitor test. For comparison, CrSe$_2$ pattern calculated from ICSD (No. 10313).
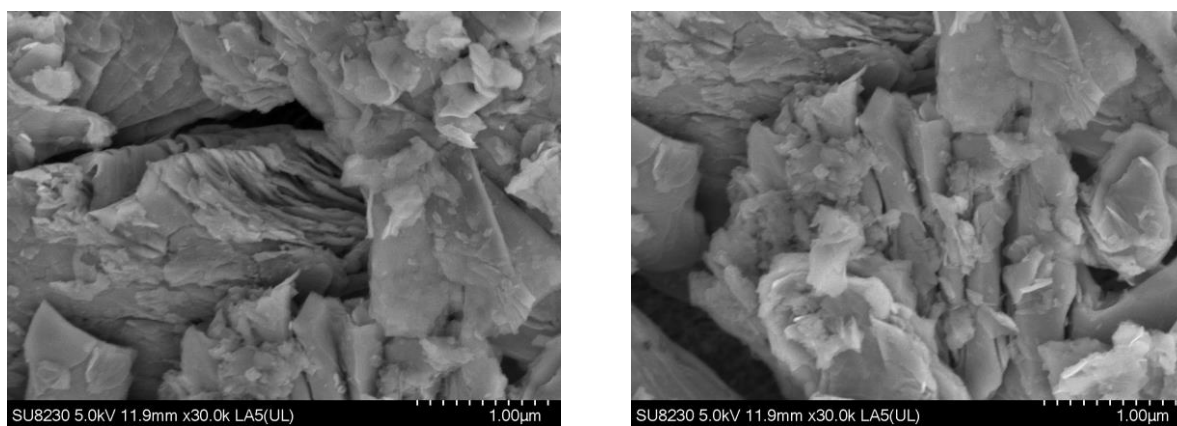

Figure. S35. The Sem image of CrSe2@G10 before (a) and after (b) multiple cycles.
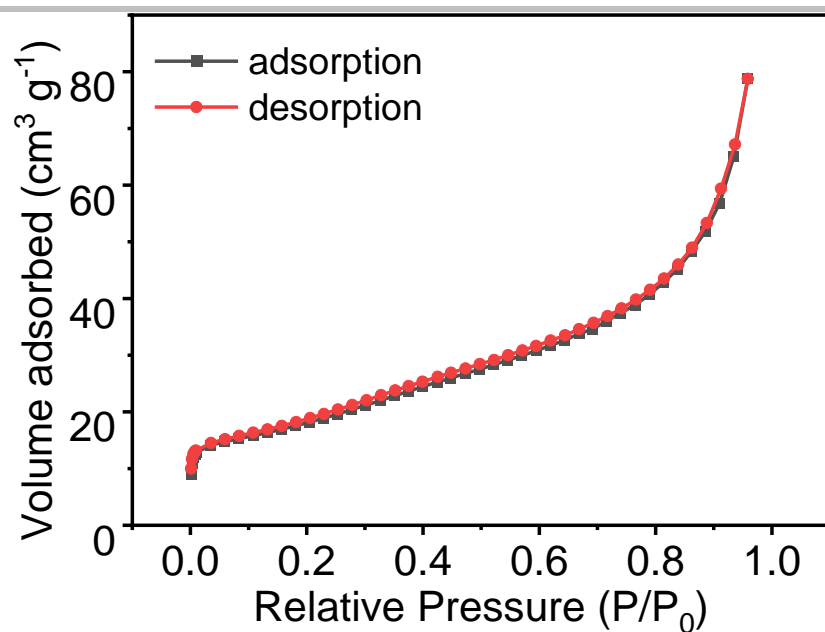
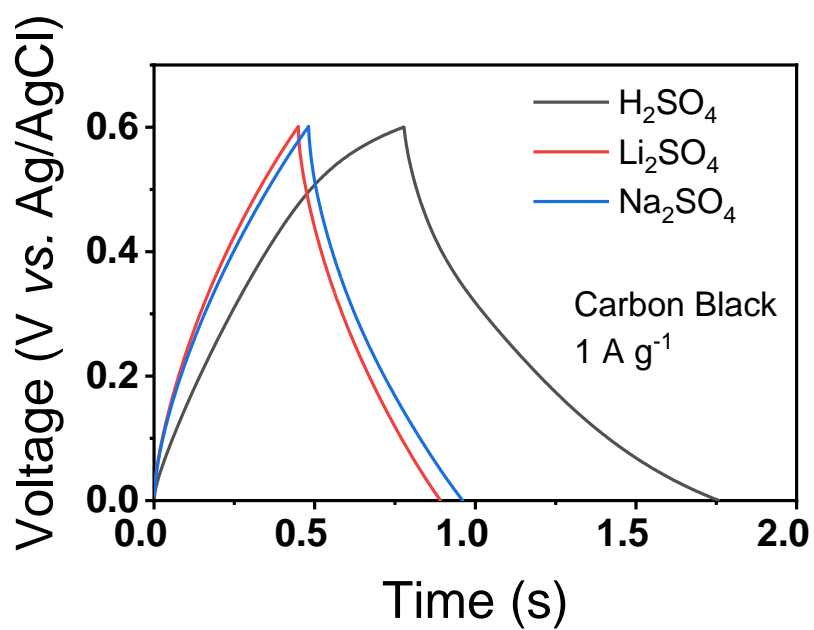**Figure S36.** Nitrogen adsorption-desorption isotherms for carbon black.

Figure S37. The GCD curves of the supercapacitor test of carbon black in three electrode system in 1 M H_2SO_4, Li_2SO_4 and Na_2SO_4 at 1 A g^{-1}.
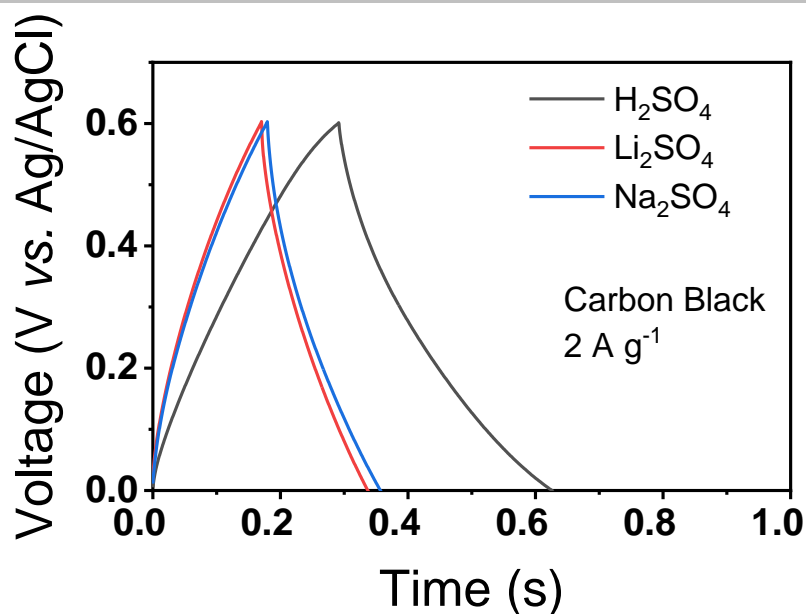
Figure S38. The GCD curves of the supercapacitor test of carbon black in three electrode system in 1 M H_2SO_4, Li_2SO_4 and Na_2SO_4 at 2 A g^{-1}.

Table S1. The summary of cell parameter of the $CrSe_2$ products determined by LeBail refinement of the experimental profile against previously reported structural model for $CrSe_2$. The standard deviations are given in parentheses.

	a, Å	c, Å	V, Å3	c/a
$CrSe_2$	3.3898(3)	5.9099(4)	58.812(9)	1.7434(2)
$CrSe_2$-G10	3.3910(3)	5.9144(3)	58.899(8)	1.7441(1)
$CrSe_2$ [4]	3.399	5.915	59.18	1.7402
$CrSe_2$ [5]	3.3908	5.9099	58.846	1.7429

Table S2. The summary of capacitance of $CrSe_2$-K and $CrSe_2$-K-G10.

	H_2SO_4	Li_2SO_4	Na_2SO_4
$CrSe_2$	3.7 F g^{-1}	0.6 F g^{-1}	0.4 F g^{-1}
$CrSe_2$-G10	27.3 F g^{-1}	9.9 F g^{-1}	7.7 F g^{-1}

Table S3. The summary of other TMDs material in supercapacitor application.

Working electrode	Electrolyte	Potential Window (V)	Specific Capacitance	Current collector	Counter electrode	Ref.
$CrSe_2$-Graphite	1M H_2SO_4	0-0.6	27.3 F g^{-1}	Ti foil	Pt foil	This work
$CrSe_2$/Ti_3C_2	3M KOH	0-0.45	80 mF cm^{-2}	Ni foam	Pt foil	[6]
VSe_2	KNO_3/PVA	0-1	4.17 mF cm^{-2}	Pt	Pt foil	[7]

VS$_2$	BMIMBF$_4$/PVA	0-0.6	4.8 mF cm^{-2}	Au	VS$_2$	[8]
MoS$_2$	1 M Na$_2$SO$_4$	-1.0 -0.2	180 F g^{-1}	Mo foil	Pt	[9]
MoSe$_2$	0.5 M H$_2$SO$_4$	0-0.8	198.9 F g^{-1}	Stainless still foil	MoSe$_2$	[10]
WS$_2$	0.1 M Na$_2$SO$_4$	-0.3-0.5	51 mF cm^{-2}	W foil	Pt foil	[11]
WSe$_2$	0.5 M KCl	0-0.6	5.1 F g^{-1}	n/a	Activated carbon	[12]
MoS$_2$	1 M Na$_2$SO$_4$	0-1.0	3.40 F g^{-1}	n/a	MoS$_2$	[13]
MoSe$_2$	1 M Na$_2$SO$_4$	0-1.0	2.57 F g$_{-1}$	n/a	MoSe$_2$	[13]
WS$_2$	1 M Na$_2$SO$_4$	0-1.0	3.50 F g^{-1}	n/a	WS$_2$	[13]
TiS$_2$	1 M Na$_2$SO$_4$	0-1.0	4.60 F g^{-1}	n/a	TiS$_2$	[13]

Supplementary Note 1

The specific capacitance was calculated using the following equation:

$$C = I \frac{\Delta t}{A\,\Delta V}$$

where I is the working current (mA), Δt is the discharging time (s), A is the total mass of the electrode (mg), and ΔV is the voltage range (V).

References

[1] B. H. Toby, R. B. Von Dreele, *J. Appl. Crystallogr.* **2013**, *46*, 544-549.
[2] C. Fang, C. Van Bruggen, R. De Groot, G. Wiegers, C. J. o. P. C. M. Haas, *J. Phys.: Condens.Matter* **1997**, *9*, 10173.
[3] J. P. Perdew, K. Burke, M. Ernzerhof, *Phys. Rev. Lett.* **1996**, *77*, 3865-3868.
[4] C. F. van Bruggen, R. J. Haange, G. A. Wiegers, D. K. G. de Boer, *Physica B+C* **1980**, *99*, 166-172.
[5] X. Song, S. N. Schneider, G. Cheng, J. F. Khoury, M. Jovanovic, N. Yao, L. M. Schoop, *Chem. Mater.* **2021**, *33*, 8070-8078.
[6] S. Raj K A, N. Barman, N. K, R. Thapa, C. S. Rout, *Sustainable Energy Fuels* **2022**, *6*, 5187-5198.
[7] C. Wang, X. Wu, Y. Ma, G. Mu, Y. Li, C. Luo, H. Xu, Y. Zhang, J. Yang, X. Tang, J. Zhang, W. Bao, C. Duan, *J. Mater. Chem. A* **2018**, *6*, 8299-8306.
[8] J. Feng, X. Sun, C. Wu, L. Peng, C. Lin, S. Hu, J. Yang, Y. Xie, *J. Am. Chem. Soc.* **2011**, *133*, 17832-17838.
[9] K. Krishnamoorthy, G. K. Veerasubramani, P. Pazhamalai, S. J. Kim, *Electrochim. Acta* **2016**, *190*, 305-312.
[10] S. K. Balasingam, J. S. Lee, Y. Jun, *Dalton Trans.* **2015**, *44*, 15491-15498.
[11] K. Sambath Kumar, N. Choudhary, D. Pandey, Y. Ding, L. Hurtado, H.-S. Chung, L. Tetard, Y. Jung, J. Thomas, *J. Mater. Chem. A* **2020**, *8*, 12699-12704.
[12] P. Iamprasertkun, W. Hirunpinyopas, V. Deerattrakul, M. Sawangphruk, C. Nualchimplee, *Nanoscale Adv.* **2021**, *3*, 653-660.
[13] M. A. Bissett, S. D. Worrall, I. A. Kinloch, R. A. W. Dryfe, *Electrochim. Acta* **2016**, *201*, 30-37.

Author Contributions